PCCP

Cite this: *Phys. Chem. Chem. Phys.*, 2011, **13**, 18468–18480

www.rsc.org/pccp

**PERSPECTIVE**

# The polymorphism of ice: five unresolved questions†

**Christoph G. Salzmann,*[a] Paolo G. Radaelli,[b] Ben Slater[c] and John L. Finney[d]**

***Received 26th May 2011, Accepted 23rd August 2011***
**DOI: 10.1039/c1cp21712g**

Our recent discovery of three new phases of ice has increased the total number of known distinct polymorphs of ice to fifteen. In this Perspective article, we give a brief account of previous work in the field, and discuss some of the particularly interesting open questions that have emerged from recent studies. These include (i) the effectiveness of acid and base dopants to enable hydrogen-ordering processes in the ices, (ii) the comparison of the calorimetric data of some of the crystalline phases of ice and low-density amorphous ice, (iii) the disagreement between the experimental ice XV structure and computational predictions, (iv) the incompleteness of some of the hydrogen order/disorder pairs and (v) the new frontiers at the high and negative pressure ends of the phase diagram.



## 1. Introduction

The water molecule is the third most abundant molecular species in the universe following dihydrogen and carbon monoxide.[1] A substantial proportion of our planet is covered by liquid water which, sometimes called the 'matrix of life' or the 'universal solvent', is thought to be essential for the evolution and support of life on Earth.[2] Most of the ice on Earth is located near the poles. The Antarctic continent, for example, is covered by about ten petatons of snow and ice.[3] The polymorph of ice that crystallises upon cooling liquid water at ambient pressure is called ice I*h* where the '*h*' indicates the hexagonal symmetry of its crystal structure, a fact that is ultimately reflected in the 6-fold rotational symmetry of snowflakes.

Ice I*h* is an unusual material in many respects.[3–5] Famously, its density is lower than the liquid, and consequently, ice I*h* floats on water. The volume decrease upon melting also causes the melting-point depression with increasing pressure. Its pronounced plastic properties under stress are responsible for the flow of glaciers.[6] Like liquid water in the 0 to 4 °C temperature range, ice I*h* exhibits negative thermal expansion in the temperature range below 70 K.[7,8] Furthermore, ice I*h* was among the first materials found to undergo pressure-induced amorphisation. Upon compression at 77 K, ice I*h* transforms to high-density amorphous ice above 1 GPa.[9,10] Pure ice I*h* is a poor conductor for direct current.[4] However, its high dielectric constant makes ice I*h* an effective capacitor and hence a conductor for alternating current.[4] Most recently, it has been suggested that ice I*h* may be an efficient hydrogen storage material.[11]

Ice I*c* or cubic ice is an apparently metastable phase of ice and is thought to exist in the upper atmosphere.[12,13] It has been suggested that Scheiner's halo, a rare halo at 28° from the sun or the moon, is due to the presence of ice I*c* in the atmosphere.[14]

The high-pressure phases of ice were some of the very first high-pressure polymorphs to be discovered.[15] In the early 20th century, Gustav Tammann and Percy W. Bridgman established the convention that newly discovered phases of ice are to be labelled with Roman numerals.[16,17] Petrenko and Whitworth argue that 'Roman numerals should only be used for crystalline phases that are experimentally well established, for example by crystallography',[4] a procedure that we think is useful to avoid confusion over the naming of phases. The most recent phase of ice, discovered in 2009, was ice XV.[18] Fig. 1 shows the up-to-date phase diagram of $H_2O$ in the pressure range up to 2.5 GPa including the region of thermodynamic stability of the most recent newcomer ice XV.[18]

It is not clear if high-pressure phases of ice exist on Earth. The thickest ice sheets fall short of the 22 kilometres required to build up pressure high enough so that ices II or III could form.[19] However, it has been suggested that ice VII may exist in cold subconducting slabs as a consequence of minerals, such as brucite, lawsonite blueschist or antigorite, undergoing dehydration reactions.[20] Also, the spectral signature consistent with ice VI, the first of the high-pressure phases with a melting point above 0 °C, has been recorded from inclusions in cuboid diamond.[21] In the solar system, high-pressure phases of ice are expected to exist in the interiors of icy planets and moons as

[a] *Department of Chemistry, Durham University, South Road, Durham DH1 3LE, UK. E-mail: c.g.salzmann@durham.ac.uk*
[b] *Department of Physics, University of Oxford, Parks Road, Oxford OX1 3PU, UK*
[c] *Department of Chemistry, University College London, 20 Gordon Street, London WC1H 0AJ, UK*
[d] *Department of Physics and Astronomy and London Centre for Nanotechnology, University College London, Gower Street, London WC1E 6BT, UK*

† This article is dedicated to the late Erwin Mayer (University of Innsbruck, Austria).

 

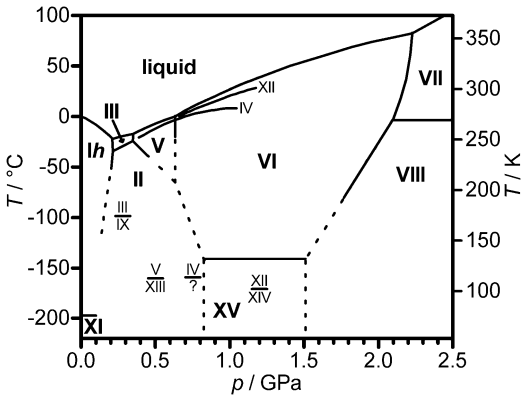


**Fig. 1** The phase diagram of water and ice including the melting lines of metastable ices IV and XII, and extrapolated phase boundaries at low temperatures (dashed lines).[4,18,110] Metastable phases are indicated by a smaller font size. This includes stable phases outside their regions of stabilities. Ice XII was assigned to the melting line shown based on the spectroscopic data in ref. 59,150.

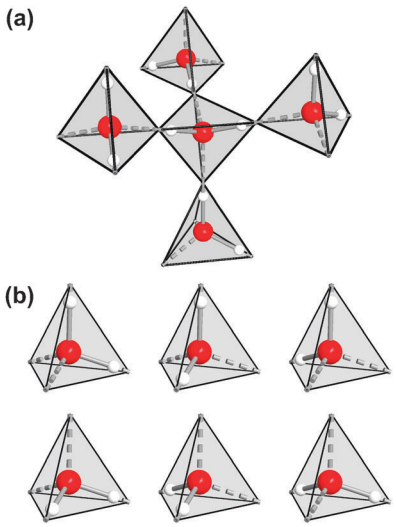


**Fig. 2** (a) A pentameric fragment of an ice I*h* structure. Each of the polyhedra contains one water molecule. Covalent bonds are indicated by solid lines and hydrogen bonds by broken lines, respectively. The corners of the polyhedra are defined by the midway position between two hydrogen-bonded oxygen atoms. (b) The six possible orientations of a water molecule in ice.

well as a consequence of meteorite impacts onto ice surfaces at low temperatures.[1,22]

In this Perspective article, we present a brief 'guided tour' through the phase diagram by introducing the various phases of ice. This is followed by a discussion of some of the open questions in the field that have emerged from recent work.

## 2. The crystal structures of the ice phases

The water molecules in the crystalline ices are fully hydrogen bonded which results in a four-fold coordination of the molecules. The exact bonding conditions are defined by the Bernal-Fowler ice rules which state that (i) one and only one hydrogen atom is found along each of the hydrogen bonds and that (ii) always two hydrogen atoms are covalently bonded to each of the oxygen atoms which preserves the stoichiometry of the $H_2O$ molecules.[23] Fig. 2(a) shows a pentameric fragment of an ice I*h* structure with a fully hydrogen-bonded water molecule in its centre. Each of the five polyhedra shown contains one water molecule, and the corners of the polyhedra are located at the midway positions between the hydrogen-bonded oxygen atoms.

The crystal structures of the various polymorphs of ice can be built up by linking such polyhedra together at their corners. Fig. 3(a–h) shows the resulting three-dimensional hydrogen-bonded network topologies of all known phases of ice. The only two phases with large open-channel structures are ice I*h* and ice II. The ice II structure can actually be thought of as 'ice nanotubes' interconnected through hydrogen bonding. It has been shown that the ice II channels can be filled with helium atoms.[24,25]

Fig. 3(i) shows the results of a ring-size analysis of the various network topologies. A ring is defined as a closed path along hydrogen-bonded water molecules without any 'shortcuts' in this context, and the size of a ring equals the number of constituting water molecules. The densities of the structures increase from top to bottom in Fig. 3(i).

Starting from only six-membered rings in ices I*h*, I*c* and XI, the average ring size increases at first as the densities of the phases increase. This goes along with an increase in the number of different ring sizes, and hence structural complexity. The most complicated crystal structures are those of ices V/XIII whose structures contain rings ranging from four to twelve-membered. Interestingly, ten-membered rings are the dominating structural features in the density range from ice II to ice IV.

The increase in density of the ice phases is achieved by bending of the hydrogen bonds as well as by the interpenetration of hydrogen-bonded networks. The ice XII/XIV network, which consists of seven and eight-membered rings, is the highest-density ice structure not containing any interpenetrating elements.[26,27] In ices V/XIII and IV, hydrogen bonds thread through rings, eight-membered rings in ices V/XIII[28,29] and six-membered rings in ice IV.[30] The water molecules that form the hydrogen bonds through the rings are not directly hydrogen bonded to any of the water molecules that constitute the rings. However, all water molecules in ices V/XIII and IV still belong to the same hydrogen-bonded network. Ices VI/XV and VII/VIII on the other hand consist of two independent interpenetrating networks not hydrogen-bonded to each other. The ice VII structure comprises two interpenetrating ice I*c* networks as is shown schematically in Fig. 3(h). The smallest average ring size observed for the ice phases is six. However, smaller average ring sizes can be found in the fully hydrogen-bonded water-networks of the various clathrate hydrates.[31]

Ices I*h* and I*c* contain only six-membered rings as shown in Fig. 3(i). The structural difference between the two lies in the stacking sequence of layers consisting of water molecules arranged as six-membered rings with the 'chair' conformation.[32–34] In ice I*h*, each layer is the mirror image of the previous layer (*cf.* Fig. 4(a)), whereas in case of ice I*c*, each successive layer is not mirrored but shifted half-way across the diagonal of the six-membered rings (*cf.* Fig. 4(b)). The stacking of the layers leads to six-membered rings with the 'boat' conformation in ice I*h*. The ice I*c* structure on the other hand contains only 'chair' six-membered rings.

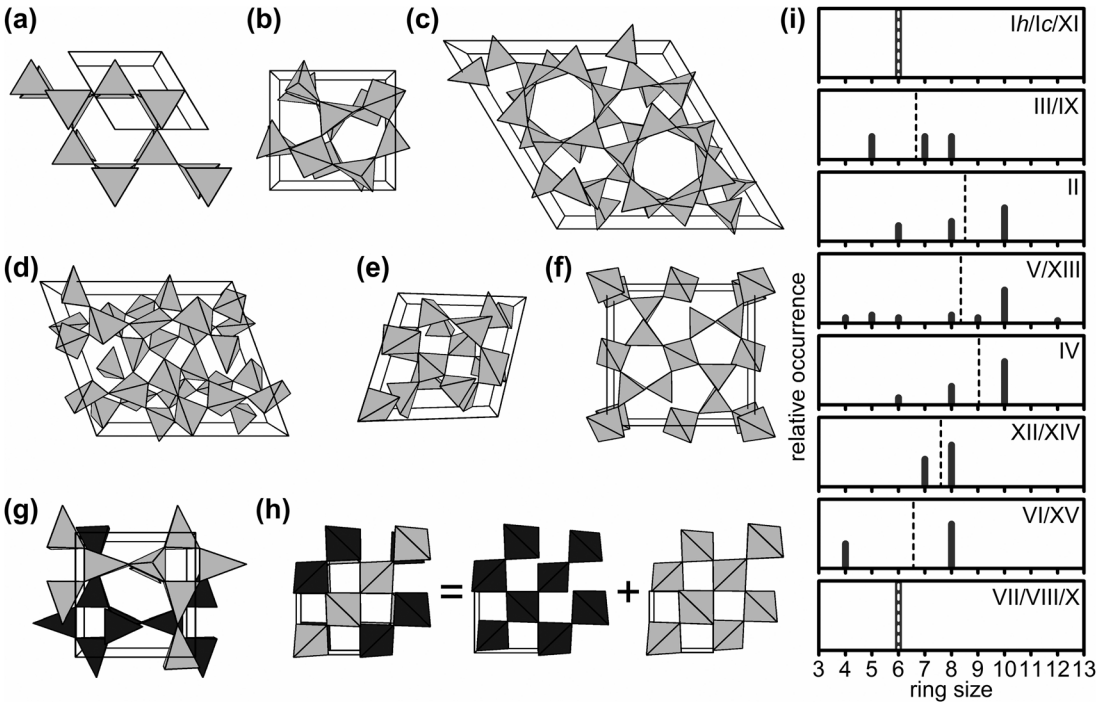


**Fig. 3** Network topologies of ice I*h* (a), ice III (b), ice II (c), ice V (d), ice IV (e), ice XII (f), ice VI (g) and ice VII (h) using the polyhedron definition of Fig. 2. The unit-cell edges are shown as solid black lines. The ice II structure (c) is shown with a hexagonal unit cell, whereas for ice IV (e) the rhombohedral unit cell was chosen. The two independent and interpenetrating networks of ices VI (g) and VII (h) are shown by dark and light polyhedra, respectively. For ice VII, the two individual ice I*c* networks are shown separately. (i) Analysis of the ring sizes in the various phases of ice. The densities of the crystal structures increase from top to bottom. The average ring sizes are indicated by dashed lines.

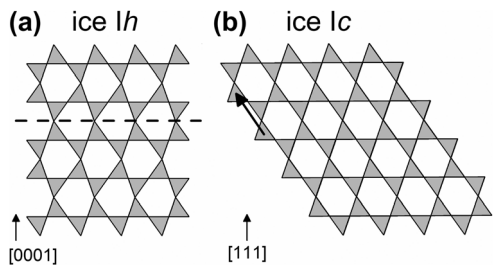


**Fig. 4** Comparison of the crystal structures and stacking of layers in ice I*h* (a) and ice I*c* (b). The polyhedra are defined as in Fig. 2. The dashed line in (a) indicates the mirror plane in between two layers, and the arrow in (b) shows the displacement vector from one layer to the next.

Due to the similar molecular environments in ice I*h* and ice I*c*, it is not possible to distinguish between the two by using infrared or Raman spectroscopy.[35,36] The structural differentiation between ice I*h* and ice I*c* is further complicated by the fact that cubic ice obtained experimentally has always contained hexagonal stacking faults. Depending on the preparation conditions and the thermal history of the sample, varying amounts of hexagonal stacking can be found.[33,37,38] The amounts of hexagonal stacking in cubic ice can be determined quantitatively from diffraction data.[39,40]

The orientations of the water molecules in ice are not necessarily fully defined. Within the limitations imposed by the Bernal-Fowler rules, a given water molecule can still adopt six different orientations as shown in Fig. 2(b). The hydrogen-disordered phases of ice display orientational disorder of the water molecules and therefore only long-range order of the oxygen atoms. Strictly speaking, such a structure cannot be treated by means of traditional crystallography. However, the approach often taken is to describe the hydrogen-disordered structures by using half-occupied hydrogen atom sites, which represent the average structure. The positional disorder of the oxygen atoms, which results from hydrogen disorder, is often neglected during structural refinements.[41] The local bond distances and angles may therefore differ from the ones deduced from the average structure.[42]

In the hydrogen-ordered phases of ice, the water molecules are only found in the energetically most favoured orientations. Consequently, these phases exhibit long-range order of both the hydrogen and the oxygen atoms, and the crystallographically determined bond distances and angles reflect the local structures.

The network structures shown in Fig. 3(a–h) can, in principle, be either hydrogen-disordered or ordered. The various phases of ice can therefore be grouped into pairs as shown in Table 1. States in between the two extremes of complete hydrogen order and disorder are also possible and can be described by using fractional occupancies of the hydrogen-atom sites either between zero and $\frac{1}{2}$, or between $\frac{1}{2}$ and one. Out of all the hydrogen-disordered phases known only two, ices III and V, have been found to exhibit partial hydrogen order.[41,43,44] For all the other disordered phases, the fractional occupancies of the hydrogen atoms were determined to be $\frac{1}{2}$.

The molecular character of the water molecule remains intact in almost all of the known phases of ice. In fact, with increasing

 

**Table 1** The various hydrogen-disorder/order pairs and the dopants required to promote the ordering transitions. The space-group symmetries of the various phases are given in parentheses.

| Hydrogen-disordered phase of ice | Hydrogen-ordered phase of ice | Dopant |
|---|---|---|
| I*h* ($P6_3/mmc$)[152] | XI ($Cmc2_1$)[75,101] | KOH (and other hydroxides) |
| I*c* ($Fd\bar{3}m$)[12,34] | ? | ? |
| III ($P4_12_12$)[16,41,43] | IX ($P4_12_12$)[91,153,154] | not required |
| ? ($R\bar{3}c$)[73] | II ($R\bar{3}$)[16,155,156] | |
| V ($A2/a$)[17,29] | XIII ($P2_1/a$)[74] | HCl, HF |
| IV ($R\bar{3}m$)[17,30,56] | ? | ? |
| XII ($I\bar{4}2d$)[26] | XIV ($P2_12_12_1$)[74] | HCl |
| VI ($P4_2/nmc$)[17,121,157] | XV ($P\bar{1}$)[18] | HCl |
| VII ($Pn\bar{3}m$)[121,158,159] | VIII ($I4_1/amd$)[96,120,121] | not required |

density of the phases, the hydrogen bonds weaken as the oxygen-oxygen distances increase due to the progressive interpenetration of networks. This is illustrated by the fact that the frequencies of the coupled and decoupled O–H and O–D stretching transitions in Raman spectroscopy increase in wavenumber with increasing densities of the phases.[45–48]

Upon compression of ice VII, the hydrogen bonds become symmetric upon increasing the pressure to about 70 GPa.[49–53] This 'polymeric' form of ice has been called ice X which, at present, is the highest-density phase of ice known. Due to its symmetric hydrogen bonds, ice X is neither hydrogen ordered nor disordered, and therefore not included in Table 1.

## 3. Phase transitions of the ice phases

Several of the ice phases can be crystallised from the liquid (*cf.* Fig. 1). These include the thermodynamically stable phases ices I*h*, III, V, VI and VII. However, it is often possible to supercool the liquid with respect to the stable phases of ice, which can result in the crystallisation of the metastable phases ices I*c*, IV and XII from the liquid.[13,26,30,54–57] The addition of nucleating agents to water can favour the crystallisation of some of the metastable ice phases.[58] This approach has been used in order to crystallise ice IV from the liquid.[56] However, even under optimised conditions, the preparation of ice IV was only successful in one attempt out of ten.[56] For this reason, ice IV has been called a 'will-o'-the-wisp, a tentative, ghostly form of ice'.[2] By contrast, the crystallisation of ice XII from the liquid seems to be more straightforward.[26,59]

In addition to crystallising the high-pressure phases of ice from the liquid, they can also be formed by heating high-density amorphous ice under pressure.[60–64] Precise control over the crystallisation pressure and the rate of heating during crystallisation allows the preparation of pure ices IV and XII, and all the other phases that can be crystallised from the liquid phase.[64] Notably, ice II, which does not have a phase boundary with the liquid phase, could not be prepared following this route.

Reconstructive phase transitions, which involve changes in the network topologies, and hence breaking and reforming of hydrogen bonds, are only observed in a relatively narrow temperature range below the liquidus lines. Several of the solid-solid phase boundaries shown in Fig. 1 are extrapolated to lower temperatures for this reason. For example, the location of the ice II/V/VI triple point can only be determined by extrapolation of the ice II/V and ice V/VI phase boundaries (*cf.* Fig. 1).[65]

The slow kinetics of the reconstructive phase transitions at low temperatures make it possible to recover and characterise several of the high-pressure phases at ambient pressure and low temperatures, typically in liquid nitrogen. These recovered phases transform irreversibly to ice I*c*[37,38,66–68] and subsequently to ice I*h* upon heating at ambient pressure.[37,38,68,69] The exceptions are ices VII and VIII, which transform to low-density amorphous ice first upon heating before also turning into ice I*c*.[70–72]

With the network topologies remaining unchanged, the phases of ice can undergo reversible phase transitions from hydrogen disorder to hydrogen order (*cf.* Fig. 1 and Table 1). Hydrogen disorder is generally found at high temperatures where enough thermal energy is available for the water molecules to explore the entire configurational manifold. Upon decreasing the temperature, the hydrogen-disordered phases are expected to undergo exothermic phase transitions to hydrogen-ordered phases as required by the 3rd law of thermodynamics. The half-occupied hydrogen sites in the hydrogen-disordered phases can give rise to high space group symmetries. The phase transition from hydrogen disorder to hydrogen order is therefore often accompanied by breaking of the space group symmetry.[18,73,74]

The hydrogen-ordered phases represent the energetic ground states for their given network topologies. Depending on the relative orientations of the dipole moments of the water molecules, the hydrogen-ordered phases of ice can be either ferroelectric, if the dipole moments add up to yield a net moment, or antiferroelectric, if the dipole moments cancel each other. So far, out of the seven hydrogen-ordered phases identified, only ice XI, the hydrogen-ordered counterpart of ice I*h*, was found to be ferroelectric.[75–79]

Linus C. Pauling estimated the molar configurational entropy of a completely hydrogen disordered phase to be $R \ln \frac{3}{2}$ (3.37 J mol$^{-1}$ K$^{-1}$).[80] Within the errors of the experiment, this value was later confirmed experimentally for ice I*h*.[81] The configurational entropy of a completely hydrogen-ordered phase of ice is zero as expected for a perfectly ordered crystal according to the 3rd law of thermodynamics. The Pauling entropy therefore also reflects the expected entropy change for the transition from complete hydrogen order to complete hydrogen disorder. Consequently, the enthalpy change for such

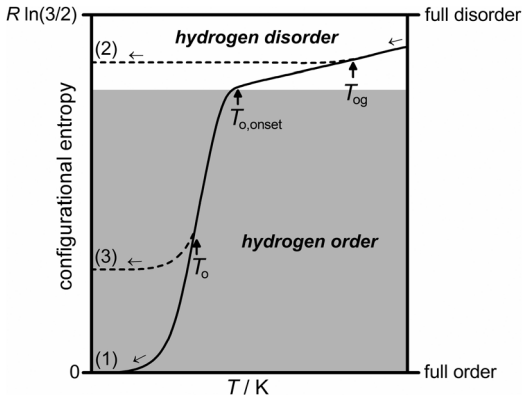


**Fig. 5** Schematic illustration of the molar configurational entropy of ice upon cooling. The thermodynamic pathway is drawn as a solid line whereas metastable pathways are depicted as dashed lines.

a phase transition is $RT_o \ln\frac{3}{2}$, where $T_o$ is the temperature of the hydrogen disorder/order phase transition.

The configurational entropy of partially hydrogen-ordered ice lies in between zero and the Pauling entropy. The exact calculation is, however, far from trivial. Building on work by Minagawa[82] and Nagle,[83–85] Howe and Whitworth derived an expression for the calculation of the configurational entropy from a single order parameter.[86] A more rigorous approach, and one which allows several order parameter to be used, was developed by MacDowell and coworkers.[87] Using their methodology, the configurational entropies of any hydrogen-disordered or partially hydrogen-ordered phase of ice can be calculated from the fractional occupancies of the hydrogen atom sites as determined by neutron diffraction.

The expected changes in configurational entropy upon cooling a hydrogen-disordered phase are shown schematically in Fig. 5 as a solid line. The onset temperature of the hydrogen ordering phase transition, $T_{o,onset}$, is different for every hydrogen order/disorder pair (*cf.* Fig. 1). For ice V/XIII it has been found calorimetrically that only 66% of the Pauling entropy is lost during the hydrogen-ordering phase transition which indicates significant 'anticipatory' ordering in the disordered phase before the ordering phase transition takes place.[41,88] For most other hydrogen-disordered phases, the pre-ordering in the disordered phase is either less pronounced or it may even not take place. In the case of ice XII it could be shown calorimetrically that weak pre-ordering takes place despite the fact that this is not detectable by diffraction.[89,90]

Having introduced the currently known phases of ice, and discussed their structures and mechanisms of preparation, we now turn to five particularly interesting questions that have arisen from recent work in the field.

## 4. Are acid or base dopants more effective in promoting hydrogen ordering?

In order for the hydrogen-ordering phase transitions to take place, the water molecules in the disordered phases must change their orientations dynamically until the ordering temperature is reached. For water molecules in ice to reorient, the constraints of the Bernal-Fowler ice rules have to be lifted locally through the formation of point defects. Without point defects, the orientation of a water molecule is essentially locked-in due to hydrogen bonding with the four neighbouring water molecules.

The two main types of point defects in ice are rotational and ionic defects.[4] For the rotational or Bjerrum defects either no hydrogen atoms (L defect) or two hydrogen atoms (D defect) are found along a hydrogen bond. Ionic defects are either $H_3O^+$ or $OH^-$ ions within the ice lattice. The rate of molecular reorientation in ice depends on the number density of these point defects and their mobility within the crystalline lattice.[41] Migrating point defects in ice essentially leave a 'trail' of water molecules behind whose orientations have been changed.

For ices III and VII, the intrinsic point defects are sufficient so that hydrogen ordering to ices IX and VIII can be observed upon cooling.[91,92] In fact, it does not seem possible experimentally to quench ices III and VII to liquid nitrogen temperature fast enough so that they do not transform to their hydrogen-ordered counterparts.[70] Ice VII has, however, been reported to have been prepared at low temperatures through compression of high-density amorphous ice or ice VI.[70,93]

For all the other hydrogen-disordered phases, the intrinsic point defects appear to be insufficient to promote hydrogen ordering at low temperatures, and hydrogen disorder is frozen-in upon cooling, which corresponds to pathway (2) in Fig. 5. During this process, ergodicity is lost, and the formation of an orientational glass is observed below $T_{og}$.[88,94]

Dielectric measurements have given detailed insights into the nature of the molecular reorientation processes in the various phases of ice.[91,95–100] Early studies under *in situ* pressure conditions by Whalley and coworkers have shown that it is possible to differentiate between hydrogen-disordered and hydrogen-ordered phases of ice on the basis of their static dielectric constants.[91,95,96] The dielectric relaxation times, $\tau$, at $-30$ °C were found to decrease from about 200 μs for ice I*h* to about 2 μs for ices III, V and VI.[95] For ice V, $\tau$ was found to bend sharply upon cooling at around 200 K, and it decreased to 1.5 s at 133 K.[100] The Arrhenius energy was found to decrease from 49.9 kJ mol$^{-1}$ at 260 K to 23.3 kJ mol$^{-1}$ at 160 K. The exact reasons for this change are unclear. However, it has been suggested that this may be due to a change-over from Bjerrum-defect diffusion at higher temperatures to ionic-defect diffusion at lower temperatures.[41] The long dielectric relaxation times at low temperatures illustrate why ice V becomes an orientational glass upon cooling and does not undergo a phase transition to its hydrogen-ordered counterpart which would only take place below $\sim$115 K as recent studies have shown.[74,88]

Extrinsic point defects in ice can be introduced by using dopants such as bases or acids.[4] Potassium hydroxide (KOH) doping was the first example where a dopant was found to promote a phase transition from hydrogen disorder to order. KOH and KOD-doped ice I*h* undergoes a phase transition to ferroelectric ice XI below 72 K for $H_2O$ and 76 K for $D_2O$.[75–79,101–106] In a typical experiment, ice XI is nucleated at a temperature somewhere between 10 to 20 degrees below the ordering temperature, which is followed by annealing at a temperature just a few degrees below the transition temperature

 

to encourage the growth of ice XI. The concentration of KOH in $H_2O$ (or KOD in $D_2O$) is typically around 0.1 mol $L^{-1}$ which corresponds to a 1 : 560 molar ratio of KOH to $H_2O$ (or KOD to $D_2O$). The resulting samples are usually phase mixtures of ices I*h* and XI. For example, Fukuzawa and coworkers obtained a weight fraction of ice XI of 59% after annealing a doped $D_2O$ sample at 70 K for 135 h.[105] Heating to temperatures above the ordering temperature leads to the disappearance of ice XI. However, the same group has very recently shown that the nucleation of ice XI is much easier from samples that have previously contained ice XI compared to freshly prepared doped ice I*h* samples.[106] They concluded that this could be due to small hydrogen-ordered domains remaining even when samples are heated well above the I*h*/XI transition temperature. These ordered domains are thought to facilitate the nucleation of ice XI upon subsequent cooling. Furthermore, it has also been argued that the strain energy at the ice I*h*/XI interface may also strongly influence the phase transition behaviour.[107]

Acid dopants were found to be ineffective in facilitating the phase transition to ice XI.[108,109] However, we found recently that doping with hydrochloric acid (HCl) is highly effective in enabling the hydrogen-disordered ices V, VI and XII to become hydrogen ordered upon cooling.[18,74,110] Using powder-neutron diffraction we solved the crystal structures of the resulting hydrogen-ordered phases ices XIII, XIV and XV.[18,74,110] The ice V/XIII and ice XII/XIV phase transitions were also investigated by using Raman spectroscopy.[47,111]

The differential scanning calorimetry (DSC) scan (1a) in Fig. 6 shows the heating of an ice XIII sample at ambient pressure. The endothermic peak centred at 115 K marks the phase transition from hydrogen-ordered ice XIII to hydrogen-disordered ice V.[88] Subsequent cooling (1b) and reheating (1c) demonstrated the reversibility of the phase transition. In fact, this was the first example of a hydrogen order/disorder phase transition where the reversibility could be demonstrated at ambient pressure without prior annealing.[88]

The kinetics of the ice V/XIII phase transition was studied by employing different cooling rates for the ice V → ice XIII phase transition and analysing the enthalpies of the phase transition upon subsequent reheating. It was shown that, depending on the cooling rate, different hydrogen-ordered states can be accessed. Upon fast cooling, the sample 'drops out' of equilibrium during the ordering phase transition as indicated, for example, by pathway (3) in Fig. 5. Slow-cooling on the other hand leads to samples that are more highly ordered. Using DSC we could also show that hydrogen-ordering in $H_2O$ ice V is faster than in $D_2O$ ice V, and that hydrochloric acid is more effective in promoting the ordering transition than hydrofluoric acid.[88] These findings were also confirmed qualitatively by using Raman spectroscopy.[111]

For the ice V/XIII and the ice VI/XV phase transitions it was shown that slow-cooling at ambient pressure leads to more hydrogen-ordered states than cooling under pressure at the same cooling rate.[18,74] The faster kinetics of hydrogen ordering at lower pressures is consistent with positive activation volumes of these processes. The ice XII/XIV phase transition was also found to be reversible at ambient pressure. However, significant hydrogen order could only be achieved after slow-cooling at 1.2 GPa.[47,74,110] The difficulty in reordering

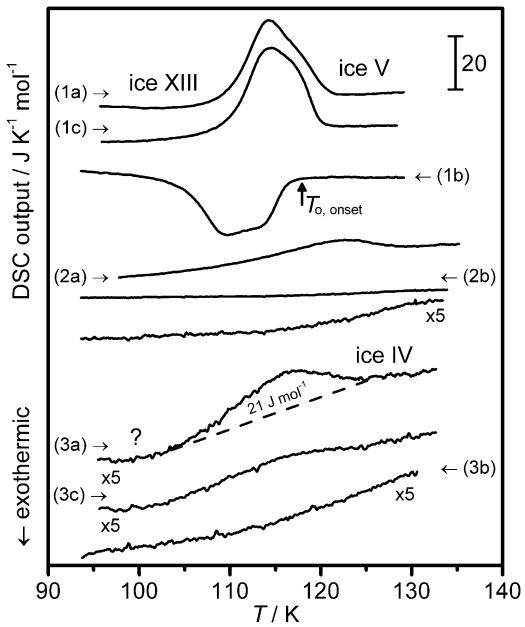


**Fig. 6** DSC scans of HCl-doped $H_2O$ ice V/XIII (1a–c), KOH-doped $H_2O$ ice V (2a,b) and HCl-doped $H_2O$ ice IV (3a–c). The direction of heating or cooling is indicated by arrows. The concentrations of the dopants in the initial sample solutions are 0.01 mol $L^{-1}$. The samples were prepared as described in ref. 18, 38, 74, 88, 110, 151 and cooled under pressure to 77 K at 1 K $min^{-1}$. Scans (1a), (2a), and (3a) show the first heating at ambient pressure at 5 K $min^{-1}$, and scans (1b), (2b) and (3b) subsequent cooling at 5 K $min^{-1}$. Scans (1c) and (3c) were recorded after cooling at 0.5 K $min^{-1}$. Scans (1a–c) and (2a,b) were adapted from ref. 88. The dashed line for scan (3a) indicates the baseline for the integration of the peak area.

ice XIV at ambient pressure was attributed to the build-up of orthorhombic stress during the tetragonal to orthorhombic phase transition.[74]

For our studies, we typically use 0.01 mol $L^{-1}$ hydrochloric acid solutions as the initial starting solutions. This corresponds to a 1 : 5600 molar ratio of HCl to $H_2O$. For the ice V/XIII phase transition, we have shown that 0.001 mol $L^{-1}$ starting solutions still yield highly ordered ice XIII samples.[88] However, the degree of hydrogen order decreased significantly upon further dilution to 0.0001 mol $L^{-1}$ suggesting that the solubility limit of HCl in ice V may lie in between those two concentrations.[88]

KOH-doped ice V samples also show an endothermic feature upon heating as shown by scan (2a) in Fig. 6 and in ref. 69. Handa and coworkers discussed this feature in terms of a hydrogen order to disorder transition. However, hydrogen order could later not be detected by Raman spectroscopy[112] or neutron diffraction.[74] We concluded that the endothermic feature originates from a relaxation effect associated with a glass-transition like behaviour around $T_{og}$ (*cf.* Fig. 5).[88] Well-relaxed samples can produce endothermic 'over-shoot' effects as the equilibrium line is crossed which is consistent with the feature of scan (2a). Higher-entropy states on the other hand can produce negative peaks in the DSC scans due to relaxation processes taking place before the equilibrium line is reached. In both cases, no latent heat is produced since the two effects are of a purely kinetic nature. The peak areas of the relaxation

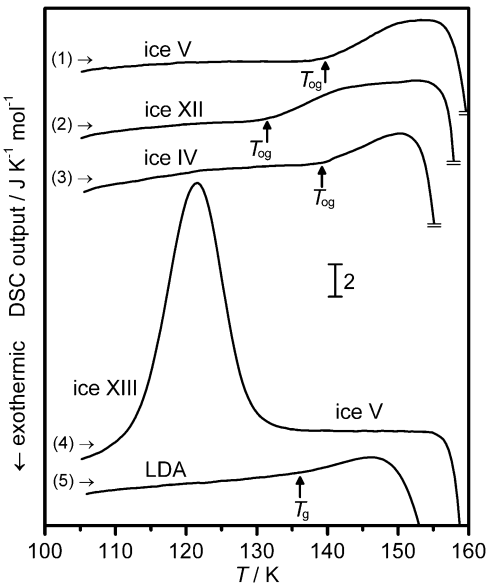


**Fig. 7** DSC scans of $H_2O$ samples of (1) ice V, (2) ice XII, (3) ice IV, (4) ice XIII and (5) low-density amorphous ice (LDA). Ice XIII is the only doped sample (0.01 mol $L^{-1}$ HCl). Ices V, XII and IV were quenched to 77 K with liquid nitrogen after the preparation under pressure,[38,89] whereas ice XIII was slow-cooled.[88] LDA was prepared from high-density amorphous ice as described in ref. 9, 89. All scans were recorded by heating at a rate of 30 K $min^{-1}$. Scans (1) and (4) were adapted from ref. 88, and scans (2) and (3) from ref. 38.

features are therefore only indirectly related to changes in entropy and hence of hydrogen order.

The ineffectiveness of KOH doping in promoting hydrogen ordering in ice V becomes apparent upon cooling (scan (2b)) where only a decrease in heat capacity is observed which starts to level off at around 120 K. Scan (1b) shows that the ordering transition to ice XIII in the case of the HCl-doped sample starts at about 117 K. This shows that, in the case of KOH-doping, the reorientation mobility freezes in on the experimental timescale just a few degrees above the onset-temperature of the ordering transition.

Curve (1) in Fig. 7 shows the DSC scan of pure ice V not containing any dopants. The step in heat capacity, which begins at about 140 K upon heating, has been linked to the glass-transition like behaviour around $T_{og}$.[88,89] The comparison of this curve with the DSC scan (2a) shown in Fig. 6 shows that KOH doping of ice V improves the reorientation dynamics, but it is not effective enough to enable the hydrogen-ordering phase transition to ice XIII.

These experiments illustrate that small differences in the effectiveness of a dopant to promote molecular reorientation in ice can decide if hydrogen ordering is observed or not on the experimental timescale. The reason for the effectiveness of HCl doping over KOH is entirely unclear, illustrating that we still know insufficient about the nature and dynamics of point defects in ice.

It is interesting to note that all the known hydrogen-ordered phases, apart from ice XI, are antiferroelectric with zero dipole moments. It is perhaps also of interest to note that the antiferroelectric phases are obtained either without any dopant or using HCl while the only ferroelectric ordered phase is obtained using KOH. Furthermore, KOH is ineffective in the formation of the antiferroelectric phases[74,88] and acid dopants are likewise ineffective in producing the one ferroelectric phase.[108,109] Although we are unaware of any experimental evidence that would bear on the reasons for these effects, it is tempting to suggest that KOH may be *inducing* the ferroelectric ice XI structure rather than catalysing the hydrogen ordering that HCl appears to be doing.

## 5. Does the calorimetric data of the crystalline phases have any relevance for amorphous ice?

Fig. 7 shows the DSC scans of pure ices V, XII and IV recorded at ambient pressure (scans (1–3)). In all three cases, endothermic steps are observed before the strongly exothermic phase transitions to ice I*c* take place. The onset-temperatures of the endothermic steps are marked by arrows in Fig. 7. These endothermic features have been shown to be reversible and have been attributed to the kinetic unfreezing of the reorientation dynamics of the water molecules.[38,88,89] In a way, these transitions can be thought of as the glass transitions of the hydrogen sublattices.

It is emphasised that such endothermic steps are not observed if the hydrogen-disordered phase is prepared from its hydrogen-ordered counterpart (*e.g.* scan (4)). In those cases, the reorientation mobility is *high* at temperatures immediately above the hydrogen-disordering phase transition. Otherwise, the hydrogen-ordering phase would not have been obtained upon cooling. The hydrogen-ordering phase transitions can therefore be used as 'probes' for testing the reorientation mobility in the ice phases.

DSC scan (5) in Fig. 7 was recorded from a low-density amorphous ice sample (LDA) which was prepared from high-density amorphous ice as described in, for example, ref. 9, 89. The scan shows the well-known increase in heat capacity at 136 K which has been assigned to the glass-transition temperature ($T_g$) of LDA.[113] According to this, LDA undergoes a transition from the glass to the highly viscous and deeply supercooled liquid above $T_g$.[113,114] However, other scenarios have been suggested as well, and it has been argued that the real glass transition of water should be at higher temperatures.[115,116] The fundamental obstacle in clarifying the situation is the fact that LDA crystallises to ice I*c* shortly above $T_g$ as can be seen in the form of the exothermic process in scan (5). The temperature range from the crystallisation temperature of LDA at the lower end to the homogeneous nucleation temperature of liquid water at the upper end has been called 'water's no-man's land'. In this temperature range, neither bulk liquid water nor LDA can be accessed.

The endothermic features of the pure crystalline ices (scans (1–3)) and LDA (scan (5)) show interesting similarities. The onset-temperatures are in a similar temperature range, and the heat-capacity increases are of comparable magnitude. Unfortunately, in the cases of LDA and ice IV, the endothermic features overlap with the crystallisation event. However, in the cases of ices V and XII, ergodicity is fully attained before the onset of crystallisation to ice I*c*. This can be seen in the form of a 'plateau' region before the phase transition to cubic ice. For ices V and XII, it has also been shown that prolonged

 

sub-$T_{og}$ annealing leads to the appearance of overshoot effects in the 'plateau' region.[89]

The similarities between the endothermic events observed for the pure crystalline phases and LDA could be taken as an indication that the underlying processes are similar and that the LDA 'glass transition' is also caused by the kinetic unfreezing of the reorientation dynamics of the water molecules. This would mean that the endothermic feature of LDA above $T_g$ is not associated with a true glass transition in the sense of a transition from the glass to the highly viscous liquid in which the molecules undergo translation diffusion processes.

The slopes of the heat-capacity increases above the $T_{og}$s are slightly higher than the slope above the $T_g$ of LDA. For further discussion of these gradients, it has to be ensured that the heat capacity increases are not affected by overshoot effects which could affect the gradient of the heat-capacity increase. For ices V and XII, this is clearly not the case, as can be seen from the appearance of the 'plateau' regions. However, for LDA and ice IV the situation is less clear since the heat-capacity increases overlap with the exotherm of the transition to cubic ice. The $\Delta C_p$ value of LDA in scan (5) is 0.7 J K$^{-1}$ mol$^{-1}$ which is thought to be close to the 'true' $\Delta C_p$ of LDA.[89,114,117] The endothermic feature in scan (5) can therefore be assumed to be free from a contribution from an overshoot effect.

The lower slope in the case of LDA could indicate that the activation of the reorientation dynamics is more difficult in LDA than it is in ices IV, V and XII. It seems possible that some of the local configurations in LDA are energetically highly unfavourable so that they are difficult to realise during the molecular reorientation processes. These unfavourable configurations could cause the associated water molecules to act as 'dead ends' for molecular reorientation processes which in turn would explain the more difficult activation of the reorientation processes in the case of LDA.

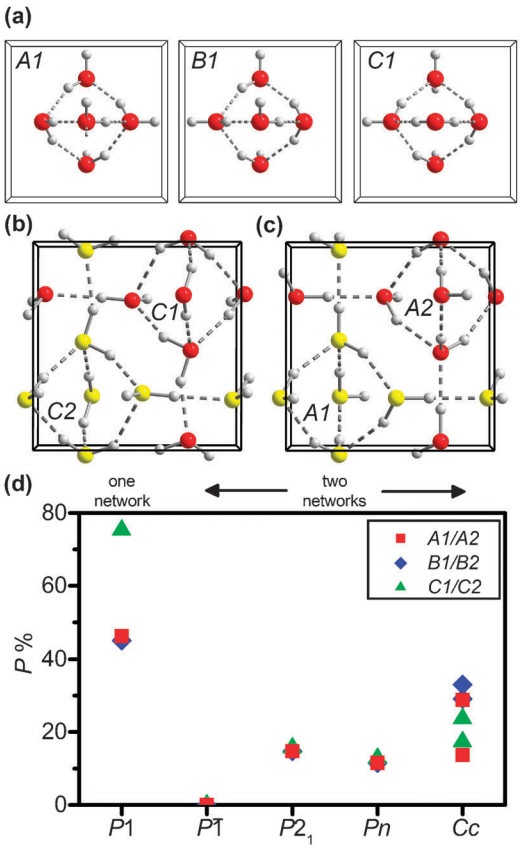


**Fig. 8** (a) Three of the six possible hydrogen-ordered structures of a single network in ice VI. The other three structures are the mirror images of the structures shown. (b) The unit-cell projection of the experimental ice XV structure[18] and (c) the structure predicted computationally.[118,119] All unit-cell projections are viewed along the *c*-direction. (d) The degrees of polarity of the various one and two network hydrogen-ordered structures.

## 6. Why do experiment and computer simulation predictions disagree in the case of ice XV?

For a given hydrogen-disordered phase there are in principle several different ways in which the disordered structure could become hydrogen ordered, including ferroelectric and antiferroelectric structures.

In the case of ice XV, the different possible ordered structures can be rationalised by first considering the ordering of one of the two individual networks of the ice VI/XV network (*cf.* Fig. 3(g)). For a single network there are six different hydrogen-ordered structures which we labelled the *A*1, *A*2, *B*1, *B*2, *C*1 and *C*2 structures.[18] The *A*1/*A*2, *B*1/*B*2 and *C*1/*C*2 pairs are related to each other by mirror symmetry. For this reason, only the *A*1, *B*1 and *C*1 structures are shown in Fig. 8(a). The ice XV structure contains two hydrogen-ordered networks. The combination of the various possible ordered networks leads to eighteen possible non-*P*1 structures containing two ordered networks. Using powder neutron diffraction we found that ice XV contains one *C*1 and one *C*2 network and that it has an overall antiferroelectric structure with $P\bar{1}$ space group symmetry (*cf.* Fig. 8(b)).[18] This suggests that the $P\bar{1}$ structure containing *C* networks is the energetic ground state, and that all other possible ordered structures are metastable with respect to this structure. Interestingly, before the experimental structure was determined, it had been predicted computationally that the lowest-energy structure should contain one *A*1 and one *A*2 network and be ferroelectric with *Cc* space group symmetry (*cf.* Fig. 8(c)).[118,119]

In order to compare the various possible ordered structures of ice XV, the degree of polarity is estimated for all possible single and double network structures. For this, a vector $\boldsymbol{d_i}$ is defined for each water molecule in the unit cell according to eqn (1).

$$\vec{d}_i = \begin{pmatrix} x_{H_1} \\ y_{H_1} \\ z_{H_1} \end{pmatrix} + \begin{pmatrix} x_{H_2} \\ y_{H_2} \\ z_{H_2} \end{pmatrix} - 2 \times \begin{pmatrix} x_O \\ y_O \\ z_O \end{pmatrix} \qquad (1)$$

These vectors point along the direction of the dipole moments of the water molecules. The degree of polarity, *P*%, of a crystal structure containing *N* water molecules per unit cell can then be calculated from eqn (2) if none of the atoms lie on corners, edges or faces of the unit cell and if only complete water molecules are contained within the unit cell. A value of 100% is obtained for an array of water molecules whose dipole

moments all point in the same direction. The $P\%$ value of an antiferroelectric structure on the other hand is zero.

$$P\% = \frac{\left|\sum_{i=1}^{N} \vec{d}_i\right|}{\sum_{i=1}^{N} \left|\vec{d}_i\right|} \times 100 \qquad (2)$$

Fig. 8(d) shows that the single-network structures of type *C* are considerably more polar than the *A* and *B* networks. The degree of polarity of the *C*1 and *C*2 networks is 75.3%. For comparison, the ice XI structure has a $P\%$ value of only 54.8%. The individual networks in ice VIII are the most polar ice structures possible since all dipole moments of the water molecules point in the same direction. The $P\%$ value is therefore 100%.

The overall degree of polarity decreases if two of the ordered ice VI networks are combined as shown in Fig. 8(d). However, only the $P\bar{1}$ space group symmetry, that of ice XV, leads to complete cancellation of the network polarities and consequently $P\%$ values of zero. All other space group symmetries yield overall ferroelectric structures.

In summary, the experimental ice XV structure contains the most polar individual networks and has the space group symmetry which allows for the most effective cancellation of the network polarities. The situation is therefore similar to ice VIII, which also contains the most polar individual networks and is antiferroeletric overall.[120,121]

Water and ice are amongst the most studied materials in the field of atomic scale simulation. Liquid water and water clusters are a perennial test bed for the accuracy of force-fields and for measuring the veracity of high level wavefunction and density functional based approaches. Force-field methods have progressed to the state where direct crystallisation of I*c* from liquid water has been achieved[122,123] and a rigid body, four site model of water has been successfully used to predict the major features of the phase diagram of ice.[124] However, capturing the energetics of hydrogen ordering in ice still presents a major challenge to force fields,[125] as multipolar electrostatic interactions dominate[126] and these are usually not adequately captured well in point-charge based models. Consequently, periodic density functional theory (DFT) based approaches have principally been used for work on characterising the hydrogen-ordered phases of ice.[126–130]

For ices II, VIII, IX, XI, XIII and XIV, the computed energetic ground state structures have been found to be in agreement with the experimental structures observed.[125–131] This implies that the experimental structures observed are indeed the relevant ground state structures. However, the computationally-predicted structure of ice XV[118,119] is at variance with that observed experimentally.[18] This disagreement prompted us to suggest that the ice XV structure could be used as a highly discriminating benchmark structure for computer modelling methods.[18]

Ice XV presents two major challenges from the first principles modelling perspective: (i) the non-bonded inter-network interactions and (ii) the large hydrogen bonding angle variance. The first point suggests that dispersion forces may be important in rationalising the relative stability of the *A*1, *A*2, *B*1, *B*2, *C*1 and *C*2 structures. On the second point, it is known that the hydrogen bonding in water clusters, for which high quality wavefunction CCSD(T) data is available for comparison as well as experimental data, is strongly influenced by the exchange–correlation functional. Our own work suggests that ordering of the *A*1, *A*2, *B*1, *B*2, *C*1 and *C*2 structures is sensitive to the proportion of Hartree–Fock exchange[132] used and the description of dispersion. With regard to dispersion, we have found that it is important to distinguish between the density on each atom using approaches such as DFT-D3[133] and vdwDF.[134] Increasing the proportion of Hartree–Fock exchange increases the degree of charge localisation and hence affects the polarisability of atoms. So, one should consider a tailored hybrid DFT approach which also includes density-responsive dispersion terms. Alternatively, very computationally demanding quantum Monte Carlo studies could also potentially resolve the hydrogen-ordering energetics of ice XV.

## 7. Which hydrogen disorder/order pairs are still incomplete?

With the recent discoveries of ices XIII, XIV and XV we identified the hydrogen-ordered counterparts of ices V, XII and VI.[18,74] However, some of the hydrogen disorder/order pairs (relating to ices I*c*, II and IV) are still incomplete as indicated by the question marks in Table 1.

Encouraged by the effectiveness of HCl doping in the previous cases, we prepared ice IV samples doped with 0.01 mol $L^{-1}$ HCl by crystallising doped high-density amorphous ice samples at 0.8 GPa and a heating rate 0.5 K $min^{-1}$ following a procedure previously developed for pure ice.[61,62] After subsequent heating to 190 K, the sample was cooled to 77 K at 1 K $min^{-1}$ under pressure, and recovered at ambient pressure in liquid nitrogen for further analysis.

Scan (3a) in Fig. 6 shows a weak endothermic feature upon first heating at ambient pressure. In order to test for reversibility, the sample was then cooled at 5 K $min^{-1}$ (scan (3b)). However, only a decrease in heat capacity could be observed which starts to level off at around 114 K. The sample was then reheated (not shown) and cooled at 0.5 K $min^{-1}$. The data recorded upon subsequent heating is shown as scan (3c). The endothermic feature was found to reappear, however, with a significantly reduced peak area compared to scan (3a). It can be concluded that slow-cooling under pressure leads to a more relaxed sample than slow-cooling at ambient pressure. The HCl doping clearly influences the reorientation dynamics within ice IV as can be seen from the comparison of scans (3a,c) in Fig. 6 and scan (3) in Fig. 7. However, it is unclear if the thermal features observed upon heating in scans (3a,c) in Fig. 6 originate from a hydrogen order to disorder transition or from the glass-transition-like behaviour of the disordered phase. Even if the thermal features were associated with a hydrogen order to disorder transition, then the degree of hydrogen order in the ordered phase would be quite small. The integrated peak area of 21 J $mol^{-1}$ from scan (3a) in Fig. 6 corresponds to an entropy change of only 5.4% of the Pauling entropy at 114 K. For now, it seems as if ice IV has transferred its 'will-o'-the-wisp' status to its hydrogen-ordered counterpart. Also, the structure of the hydrogen-ordered counterpart of ice IV has not yet been predicted computationally.

Ice I*c* is sometimes referred to as being the real ice analogue of the spin-ice state in frustrated magnetic pyrochlore materials.[135]

 

However, it should be stressed that 100% 'perfect' cubic ice, *i.e.* without hexagonal stacking faults, has actually never been prepared. Perfect cubic ice would have the same space group as diamond, and the asymmetric unit would only contain one oxygen atom and one hydrogen atom which would mean that all hydrogen bonds in perfect ice I*c* are symmetry-equivalent.[34] The phase transition to the hydrogen-ordered counterpart would therefore have to go along with signficant breaking of symmetry. Among other ordered structures, hydrogen-ordered ice I*c* could have the same structure as one of the individual networks in ice VIII, which would make it the most polar ice structure possible.

Ice II is the only hydrogen-ordered phase of ice for which the hydrogen-disordered counterpart has not been identified (*cf.* Table 1). Remarkably, ice II transforms to either ice III or ice V upon heating rather than undergoing a phase transition to its hydrogen-disordered counterpart. The reason for this is most likely that the hydrogen-ordered structure of ice II is energetically much more stable than all the other possible ordered configurations. In fact, it has recently been shown by first-principles calculations[131] that the energy difference between the ground state and the next most favourable hydrogen-ordered structure is more than an order of magnitude greater for ice II than it is for ice I*h*, perhaps providing a clue to its reluctance to hydrogen disorder.

It is intriguing to imagine the consequences if ice II transformed to a hydrogen-disordered phase in a similar temperature range as the other hydrogen-ordered phases in this pressure range of the phase diagram (*cf.* Fig. 1).[136] Above the transition temperature, the disordered ice II phase would be more stable than ices III and V, and therefore stable up to its liquidus line, which would be higher in temperature than the liquidus lines of ices III and V. This would remove the stability regions of ices III and V from the phase diagram altogether, and would most likely reduce the areas of stability of ices I*h* and VI. This example illustrates the influence of the phenomenon of hydrogen disorder/order on the overall appearance of the phase diagram. In this context it is interesting to recall the statement of Whalley and Davidson in their 1965 paper that 'the complexity of the phase diagram of ice is due largely to ice II being ordered at all temperatures.'[136]

## 8. What are the new frontiers in the exploration of the phase diagram?

The recent discovery of ice XV has completed the phase diagram in the low and medium pressure range in the sense that all regions of stability have now been mapped.[18] However, this does not exclude the possibility of finding new metastable phases in this pressure range. In the pressure range up to about 1 GPa in particular there are a large number of phases close together in free energy. The discovery of new metastable polymorphs in this pressure range would therefore seem entirely possible. In fact, the existence of a quartz-like polymorph of ice has been suggested[137,138] as well as an ice structure isomorphic to the silicate nonasil.[138] There is also the so-called, as yet unidentified, 'yellow' phase observed by Lobban.[139]

The negative-pressure region of the phase diagram is still largely uncharted territory. It has been suggested that the empty *sII* and *sH* clathrate hydrate structures could be stable under negative pressure conditions.[140] However, so far, only the properties of liquid water have been investigated at negative pressures.[141,142]

The highest pressures achieved experimentally so far in the phase diagram of ice reached 210 GPa.[53] Computationally, it has been predicted that ice VII should undergo a phase transition to a plastic or rotator phase upon heating under pressure (*e.g.* at 590 K at 10 GPa).[143,144] In this phase, the water molecules perform facile rotations within the crystalline lattice. At temperatures above approximately 2000 K, high-pressure ice is thought to transform to a superionic phase in which the hydrogen atoms become mobile while the oxygen atoms stay at fixed positions.[145–147]

A variety of post-ice X phases have been proposed computationally including high-pressure ice phases with *Pbcm*[148] and *Pbca* space group symmetries as well as a metallic *Cmcm* phase.[149] All of these phases are, like ices VII, VIII and X, based on a body centred cubic arrangement of the oxygen atoms. In ice X as well as in the *Pbcm* and *Pbca* phases the hydrogen atoms reside on sites located midway between the next-neighbour oxygen atoms. However, in the *Cmcm* phase, which is predicted to form above 1550 GPa, the hydrogen atoms are 'squeezed' into the octahedral sites of the bcc lattice.[149] These sites are located midway between the second-nearest neighbour oxygen atoms. In ice X and the *Pbcm* and *Pbca* phases, the hydrogen sites are fully occupied. However, the ratio of oxygen atoms to octahedral sites in a bcc lattice is 2 : 6. This means that only two out of three octahedral sites are occupied by hydrogen atoms in the *Cmcm* phase. It was found computationally that two vacant sites are never adjacent to one another which results in an ordered structure overall.[149] It is interesting to note that while the phenomenon of hydrogen disorder/order seemed to disappear with the formation of symmetric hydrogen bonds in ice X, with the occupation of the octahedral sites by the hydrogen atoms in the *Cmcm* phase, the phenomenon could reappear again at very high pressures. However, in this a case, a hydrogen-disordered site would exhibit a fractional occupancy of $\frac{2}{3}$ rather than the familiar value of $\frac{1}{2}$.

## Conclusions

The phase diagram of water and ice has been explored for more than a century, and research in the area has been at the forefront of research into high-pressure polymorphism. Since 2009, we know of fifteen distinct polymorphs of ice.[18] For ice XV it was found that the experimental crystal structure disagrees with the structure predicted by computational calculations.[118,119] We therefore suggested that the crystal structure of ice XV could be taken as a benchmark structure for testing and improving the computer models of water.[18]

It seems likely that the number of phases of ice will increase further in the future. The next phase of ice to be discovered could be one of the missing phases of the known hydrogen order/disorder pairs or a new metastable phase in the low and medium pressure range. Such a phase would most likely be part of a new hydrogen disorder/order pair. Furthermore, a variety of new phases have been predicted to form at the experimentally unexplored negative and very high-pressure ends of the phase diagram.

Our recent work on the hydrogen-ordered phases of ice has illustrated once more that we still do not know enough about the defect dynamics and structural relaxation processes in the various forms of ice. For example, whereas acid doping has been used successfully to prepare the hydrogen-ordered phases XIII, XIV and XV,[18,74] it was found to be ineffective in facilitating the phase transition from ice I*h* to ice XI.[102,109] Furthermore, we have shown that the calorimetric data of the pure crystalline ices IV, V and XII show interesting similarities with the endothermic feature above 136 K in the DSC scan of LDA which has been attributed to its glass transition.[113,114] In case of the crystalline phases, we have concluded that the endothermic features arise from the kinetic unfreezing of the reorientation dynamics of the water molecules.[38,88,89] This now raises the question if similar processes are responsible for the endothermic feature exhibited by LDA. We conclude that, at present, there is still no widely accepted explanation for the heat-capacity increase at 136 K in LDA. It is hoped that the comparison of the calorimetric data of LDA and the crystalline ices made here may add new fuel to the on-going debate about the glass-transition behaviour of LDA.

## Acknowledgements

We are grateful to the ISIS Facility and the Institut Laue-Langevin for access to neutron scattering facilities.

## Notes and references


1 S. Kwok, *Physics and Chemistry of the Interstellar Medium*, University Science Books, Sausalito, USA, 2007.
2 P. Ball, *$H_2O$ A biography of water*, Weidenfeld & Nicolson, 1999.
3 D. Eisenberg and W. Kauzmann, *The Structure and Properties of Water*, Plenum Press, Oxford, 1969.
4 V. F. Petrenko and R. W. Whitworth, *Physics of Ice*, Oxford University Press, Oxford, 1999.
5 P. V. Hobbs, *Ice Physics*, Clarendon Press, Oxford, 1974.
6 F. Louchet, *C. R. Phys.*, 2004, **5**, 687–698.
7 M. Jakob and S. Erk, *Wiss. Abh. Phys. Techn. Reichsanst.*, 1929, **12**, 302–316.
8 K. Röttger, A. Endriss, J. Ihringer, S. Doyle and W. F. Kuhs, *Acta Crystallogr., Sect. B: Struct. Sci.*, 1994, **50**, 644–648.
9 O. Mishima, L. D. Calvert and E. Whalley, *Nature*, 1984, **310**, 393–395.
10 O. Mishima, L. D. Calvert and E. Whalley, *Nature*, 1985, **314**, 76–78.
11 T. A. Pascal, C. Boxe and W. A. Goddard, *J. Phys. Chem. Lett.*, 2011, **2**, 1417–1420.
12 H. König, *Z. Kristallogr.*, 1943, **105**, 279–286.
13 B. J. Murray, D. A. Knopf and A. K. Bertram, *Nature*, 2005, **434**, 202–205.
14 E. Whalley, *Science*, 1981, **211**, 389–390.
15 P. McMillan, *Nat. Mater.*, 2005, **4**, 715–718.
16 G. Tammann, *Ann. Phys.*, 1900, **307**, 1–31.
17 P. W. Bridgman, *Proc. Am. Acad. Arts Sci.*, 1912, **47**, 441–558.
18 C. G. Salzmann, P. G. Radaelli, E. Mayer and J. L. Finney, *Phys. Rev. Lett.*, 2009, **103**, 105701.
19 B. Kamb, *Math. Sci. Eng.*, 1967, **31**, 27–33.
20 C. R. Bina and A. Navrotsky, *Nature*, 2000, **408**, 844–847.
21 H. Kagi, R. Lu, P. Davidson, A. F. Goncharov, H. K. Mao and R. J. Hemley, *Mineral. Mag.*, 2000, **64**, 1089–1097.
22 F. Sohl, T. Spohn, D. Breuer and K. Nagel, *Icarus*, 2002, **157**, 104–119.
23 J. D. Bernal and R. H. Fowler, *J. Chem. Phys.*, 1933, **1**, 515–549.
24 D. Londono, W. F. Kuhs and J. L. Finney, *Nature*, 1988, **332**, 141–142.
25 C. Lobban, J. L. Finney and W. F. Kuhs, *J. Chem. Phys.*, 2002, **117**, 3928–3934.
26 C. Lobban, J. L. Finney and W. F. Kuhs, *Nature*, 1998, **391**, 268–270.
27 M. O'Keeffe, *Nature*, 1998, **392**, 879.
28 E. Whalley, ed. P. Schuster, G. Zundel and C. Sandorfy, North-Holland Publishing Company, Amsterdam, 1976, vol. 3.
29 B. Kamb, A. Prakash and C. Knobler, *Acta Crystallogr.*, 1967, **22**, 706–715.
30 H. Engelhardt and B. Kamb, *J. Chem. Phys.*, 1981, **75**, 5887–5899.
31 J. S. Loveday and R. J. Nelmes, *Phys. Chem. Chem. Phys.*, 2008, **10**, 937–950.
32 L. G. Dowell and A. P. Rinfret, *Nature*, 1960, **188**, 1144–1148.
33 G. P. Arnold, E. D. Finch, S. W. Rabideau and R. G. Wenzel, *J. Chem. Phys.*, 1968, **49**, 4365–4369.
34 W. F. Kuhs, D. V. Bliss and J. L. Finney, *J. Phys. Colloq., C1*, 1987, **48**, 631–636.
35 J. E. Bertie and E. Whalley, *J. Chem. Phys.*, 1964, **40**, 1637–1645.
36 M. J. Taylor and E. Whalley, *J. Chem. Phys.*, 1964, **40**, 1660–1664.
37 I. Kohl, E. Mayer and A. Hallbrucker, *J. Phys. Chem. B*, 2000, **104**, 12102–12104.
38 C. G. Salzmann, E. Mayer and A. Hallbrucker, *Phys. Chem. Chem. Phys.*, 2004, **6**, 1269–1276.
39 T. C. Hansen, M. M. Koza and W. F. Kuhs, *J. Phys.: Condens. Matter*, 2008, **20**, 285104.
40 T. C. Hansen, M. M. Koza, P. Lindner and W. F. Kuhs, *J. Phys.: Condens. Matter*, 2008, **20**, 285105.
41 C. Lobban, J. L. Finney and W. F. Kuhs, *J. Chem. Phys.*, 2000, **112**, 7169–7180.
42 W. F. Kuhs and M. S. Lehmann, in *Science Reviews 2*, ed. F. Franks, Cambridge University Press, 1986, vol. 2, pp. 1–65.
43 J. D. Londono, W. F. Kuhs and J. L. Finney, *J. Chem. Phys.*, 1993, **98**, 4878–4888.
44 W. F. Kuhs, C. Lobban and J. L. Finney, *Rev. High Pressure Sci. Technolog.*, 1998, **7**, 1141–1143.
45 B. Minceva-Sukarova, W. F. Sherman and G. R. Wilkinson, *J. Phys. C: Solid State Phys.*, 1984, **17**, 5833–5850.
46 B. Minceva-Sukarova, G. E. Slark, W. F. Sherman and G. R. Wilkinson, *Journal de Physique*, 1987, **Colloque C1**, 37–43.
47 C. G. Salzmann, A. Hallbrucker, J. L. Finney and E. Mayer, *Chem. Phys. Lett.*, 2006, **429**, 469–473.
48 C. G. Salzmann, I. Kohl, T. Loerting, E. Mayer and A. Hallbrucker, *J. Phys. Chem. B*, 2003, **107**, 2802–2807.
49 F. H. Stillinger and K. S. Schweitzer, *J. Phys. Chem.*, 1983, **87**, 4281–4288.
50 A. Polian and M. Grimsditch, *Phys. Rev. Lett.*, 1984, **52**, 1312–1314.
51 J. Teixeira, *Nature*, 1998, **392**, 232–233.
52 A. F. Goncharov, V. V. Struhkin, M. Ho-kwang and R. J. Hemley, *Phys. Rev. Lett.*, 1999, **83**, 1998–2001.
53 A. F. Goncharov, V. V. Struzhkin, M. S. Somayazulu, R. J. Hemley and H. K. Mao, *Science*, 1996, **273**, 218–220.
54 E. Mayer and A. Hallbrucker, *Nature*, 1987, **325**, 601–602.
55 I.-M. Chou and H. T. Haselton, *Rev. High Pressure Sci. Technol.*, 1998, **7**, 1132–1134.
56 H. Engelhardt and E. Whalley, *J. Chem. Phys.*, 1972, **56**, 2678–2684.
57 K. Nishibata, *Jpn. J. Appl. Phys.*, 1972, **11**, 1701–1708.
58 L. F. Evans, *J. Appl. Phys.*, 1967, **38**, 4930–4932.
59 I.-M. Chou, J. G. Blank, A. F. Goncharov, H.-K. Mao and R. J. Hemley, *Science*, 1998, **281**, 809–812.
60 T. Loerting, I. Kohl, C. Salzmann, E. Mayer and A. Hallbrucker, *J. Chem. Phys.*, 2002, **116**, 3171–3174.
61 C. G. Salzmann, T. Loerting, I. Kohl, E. Mayer and A. Hallbrucker, *J. Phys. Chem. B*, 2002, **106**, 5587–5590.
62 C. G. Salzmann, T. Loerting, I. Kohl, E. Mayer and A. Hallbrucker, *Can. J. Phys.*, 2003, **81**, 25–32.
63 S. Klotz, G. Hamel, J. S. Loveday, R. J. Nelmes and M. Guthrie, *Z. Kristallogr.*, 2003, **218**, 117–122.
64 C. G. Salzmann, E. Mayer and A. Hallbrucker, *Phys. Chem. Chem. Phys.*, 2004, **6**, 5156–5165.
65 O. Mishima and S. Endo, *J. Chem. Phys.*, 1980, **73**, 2454–2456.
66 J. E. Bertie, L. D. Calvert and E. Whalley, *J. Chem. Phys.*, 1963, **38**, 840–846.
67 J. E. Bertie, L. D. Calvert and E. Whalley, *Can. J. Chem.*, 1964, **42**, 1373–1378.


 

68 Y. P. Handa, D. D. Klug and E. Whalley, *Can. J. Chem.*, 1988, **66**, 919–924.
69 Y. P. Handa, D. D. Klug and E. Whalley, *J. Phys. Colloq.*, 1987, **48**, 435–440.
70 S. Klotz, J. M. Besson, G. Hamel, R. J. Nelmes, J. S. Loveday and W. G. Marshall, *Nature*, 1999, **398**, 681–684.
71 D. D. Klug, Y. P. Handa, J. S. Tse and E. Whalley, *J. Chem. Phys.*, 1989, **90**, 2390–2392.
72 S. Klotz, T. Strässle, C. G. Salzmann, J. Philippe and S. F. Parker, *Europhys. Lett.*, 2005, **72**, 576–582.
73 B. Kamb, in *Physics and Chemistry of Ice*, ed. E. Whalley, S. J. Jones and L. W. Gold, Royal Society of Canada, 1973.
74 C. G. Salzmann, P. G. Radaelli, A. Hallbrucker, E. Mayer and J. L. Finney, *Science*, 2006, **311**, 1758–1761.
75 A. J. Leadbetter, R. C. Ward, J. W. Clark, P. A. Tucker, T. Matsuo and H. Suga, *J. Chem. Phys.*, 1985, **82**, 424–428.
76 R. Howe and R. W. Whitworth, *J. Chem. Phys.*, 1989, **90**, 4450–4453.
77 C. M. B. Line and R. W. Whitworth, *J. Chem. Phys.*, 1996, **104**, 10008–10013.
78 S. M. Jackson, V. M. Nield, R. W. Whitworth, M. Oguro and C. C. Wilson, *J. Phys. Chem. B*, 1997, **101**, 6142–6145.
79 S. M. Jackson and R. W. Withworth, *J. Chem. Phys.*, 1995, **103**, 7646–7647.
80 L. Pauling, *J. Am. Chem. Soc.*, 1935, **57**, 2680–2684.
81 W. F. Giauque and J. W. Stout, *J. Am. Chem. Soc.*, 1936, **58**, 1144–1150.
82 I. Minagawa, *J. Phys. Soc. Jpn.*, 1981, **50**, 3669–3676.
83 J. F. Nagle, *J. Math. Phys.*, 1966, **7**, 1484–1491.
84 J. F. Nagle, in *Physics and Chemistry of Ice*, ed. E. Whalley, S. J. Jones and L. W. Gold, Royal Society of Canada, 1973.
85 K. Nishibata and E. Whalley, *J. Chem. Phys.*, 1974, **60**, 3189–3194.
86 R. Howe and R. W. Withworth, *J. Chem. Phys.*, 1987, **86**, 6443–6445.
87 L. G. MacDowell, E. Sanz, C. Vega and J. L. F. Abascal, *J. Chem. Phys.*, 2004, **121**, 10145–10158.
88 C. G. Salzmann, P. G. Radaelli, J. L. Finney and E. Mayer, *Phys. Chem. Chem. Phys.*, 2008, **10**, 6313–6324.
89 C. G. Salzmann, I. Kohl, T. Loerting, E. Mayer and A. Hallbrucker, *Phys. Chem. Chem. Phys.*, 2003, **5**, 3507–3517.
90 M. Koza, H. Schober, A. Tölle, F. Fujara and T. Hansen, *Nature*, 1999, **397**, 660–661.
91 E. Whalley, J. B. R. Heath and D. W. Davidson, *J. Chem. Phys.*, 1968, **48**, 2362–2370.
92 P. Pruzan, J. C. Chervin and B. Canny, *J. Chem. Phys.*, 1992, **97**, 718–721.
93 R. J. Hemley, L. C. Chen and H. K. Mao, *Nature*, 1989, **338**, 638–640.
94 H. Suga, *Thermochim. Acta*, 1997, **300**, 117–126.
95 G. J. Wilson, R. K. Chan, D. W. Davidson and E. Whalley, *J. Chem. Phys.*, 1965, **43**, 2384–2391.
96 E. Whalley, D. W. Davidson and J. B. R. Heath, *J. Chem. Phys.*, 1966, **45**, 3976–3982.
97 S. R. Gough and D. W. Davidson, *J. Chem. Phys.*, 1970, **52**, 5442–5449.
98 G. P. Johari, A. Lavergne and E. Whalley, *J. Chem. Phys.*, 1974, **61**, 4292–4300.
99 G. P. Johari and E. Whalley, *J. Chem. Phys.*, 1979, **70**, 2094–2097.
100 G. P. Johari and E. Whalley, *J. Chem. Phys.*, 2001, **115**, 3274–3280.
101 Y. Tajima, T. Matsuo and H. Suga, *Nature*, 1982, **299**, 810–812.
102 Y. Tajima, T. Matsuo and H. Suga, *J. Phys. Chem. Solids*, 1984, **45**, 1135–1144.
103 T. Matsuo and H. Suga, *J. Phys.*, 1987, **C1**, 477–483.
104 H. Fukazawa, A. Hoshikawa, H. Yamauchi, Y. Yamaguchi and Y. Ishii, *J. Cryst. Growth*, 2005, **282**, 251–259.
105 H. Fukazawa, A. Hoshikawa, Y. Ishii, B. C. Chakoumakos and J. A. Fernandez-Baca, *Astrophys. J.*, 2006, **652**, L57–L60.
106 M. Arakawa, H. Kagi, J. A. Fernandez-Baca, B. C. Chakoumakos and H. Fukazawa, *Geophys. Res. Lett.*, 2011, **38**, L16101.
107 G. P. Johari, *J. Chem. Phys.*, 1998, **109**, 9543–9548.
108 M. Ueda, T. Matsuo and H. Suga, *J. Phys. Chem. Solids*, 1982, **43**, 1165–1172.
109 H. Suga, *Pure Appl. Chem.*, 1988, **55**, 427–436.
110 C. G. Salzmann, P. G. Radaelli, A. Hallbrucker, E. Mayer and J. L. Finney, in *Physics and Chemistry of Ice*, ed. W. F. Kuhs, The Royal Society of Chemistry, Cambridge, 2007, pp. 521–528.
111 C. G. Salzmann, A. Hallbrucker, J. L. Finney and E. Mayer, *Phys. Chem. Chem. Phys.*, 2006, **8**, 3088–3093.
112 B. Minceva-Sukarova, G. Slark and W. F. Sherman, *J. Mol. Struct.*, 1988, **175**, 289–293.
113 G. P. Johari, A. Hallbrucker and E. Mayer, *Nature*, 1987, **330**, 552–553.
114 I. Kohl, L. Bachmann, E. Mayer, A. Hallbrucker and T. Loerting, *Nature*, 2005, **435**, E1.
115 Y. Yue and C. A. Angell, *Nature*, 2004, **427**, 717–720.
116 C. A. Angell, *Science*, 2008, **319**, 582.
117 Y. P. Handa and D. D. Klug, *J. Phys. Chem.*, 1988, **92**, 3323–3325.
118 C. Knight and S. J. Singer, *J. Phys. Chem. B*, 2005, **109**, 21040–21046.
119 J.-L. Kuo and W. F. Kuhs, *J. Phys. Chem. B*, 2006, **110**, 3697–3703.
120 J. D. Jorgensen, R. A. Beyerlein, N. Watanabe and T. G. Worlton, *J. Chem. Phys.*, 1984, **81**, 3211–3214.
121 W. F. Kuhs, J. L. Finney, C. Vettier and D. V. Bliss, *J. Chem. Phys.*, 1984, **81**, 3612–3623.
122 M. Matsumoto, S. Saito and I. Ohmine, *Nature*, 2002, **416**, 409–413.
123 D. Quigley and P. M. Rodger, *J. Chem. Phys.*, 2008, **128**, 154518.
124 E. Sanz, C. Vega, J. L. F. Abascal and L. G. MacDowell, *Phys. Rev. Lett.*, 2004, **92**, 255701.
125 T. K. Hirsch and L. Ojamäe, *J. Phys. Chem. B*, 2004, **108**, 15856.
126 G. A. Tribello and B. Slater, *Chem. Phys. Lett.*, 2006, **425**, 246–250.
127 C. Knight, S. J. Singer, J.-K. Kuo, T. K. Hirsch, L. Ojamäe and M. L. Klein, *Phys. Rev. E: Stat., Nonlinear, Soft Matter Phys.*, 2006, **73**, 056113.
128 C. Knight and S. J. Singer, *J. Chem. Phys.*, 2008, **129**, 164513.
129 G. A. Tribello, B. Slater and C. G. Salzmann, *J. Am. Chem. Soc.*, 2006, **128**, 12594–12595.
130 C. Knight and S. J. Singer, *J. Chem. Phys.*, 2006, **125**, 064506.
131 X. Fan, D. Bing, J. Zhang, Z. Shen and J.-K. Kuo, *Comput. Mater. Sci.*, 2010, **49**, S170–S175.
132 G. A. Tribello, A. M. Walker, F. Cora, J. D. Gale, C. G. Salzmann and B. Slater, 2011, in preparation.
133 S. Grimme, J. Antony, S. Ehrlich and H. Kriege, *J. Chem. Phys.*, 2010, **132**, 154104.
134 M. Dion, H. Rydberg, E. Schroder, D. C. Langreth and B. L. Lundquist, *Phys. Rev. Lett.*, 2004, **92**, 246401.
135 S. T. Bramwell and M. J. P. Gingras, *Science*, 2001, **294**, 1495–1501.
136 E. Whalley and D. W. Davidson, *J. Chem. Phys.*, 1965, **43**, 2148–2149.
137 I. M. Stishchev and P. G. Kusalik, *Phys. Rev. B*, 1996, **53**.
138 G. A. Tribello, B. Slater, M. A. Zwijnenburg and R. G. Bell, *Phys. Chem. Chem. Phys.*, 2010, **12**, 8597–8606.
139 C. Lobban, *PhD thesis*, University College London, 1998.
140 M. M. Conde, C. Vega, G. A. Tribello and B. Slater, *J. Chem. Phys.*, 2009, **131**, 034510.
141 J. L. Green, D. J. Durben, G. H. Wolf and C. A. Angell, *Science*, 1990, **249**, 649–652.
142 Q. Zheng, D. J. Durben, G. H. Wolf and C. A. Angell, *Science*, 1991, **254**, 829–832.
143 Y. Takii, K. Koga and H. Tanaka, *J. Chem. Phys.*, 2008, **128**, 204501.
144 J. L. Aragones, M. M. Conde, E. G. Noya and C. Vega, *Phys. Chem. Chem. Phys.*, 2009, **11**, 543–555.
145 C. Cavazzoni, G. L. Chiarotti, S. Scandolo, E. Tosatti, M. Bernasconi and M. Parrinello, *Science*, 1999, **283**, 44–46.
146 A. F. Goncharov, N. Goldman, L. E. Fried, J. C. Crowhurst, I.-F. W. Kuo, C. J. Mundy and J. M. Zaug, *Phys. Rev. Lett.*, 2005, **94**, 125508.
147 T. R. Mattson and M. P. Desjarlais, *Phys. Rev. Lett.*, 2006, **97**, 017801.
148 M. Benoit, M. Bernasconi, P. Rocher and M. Parrinello, *Phys. Rev. Lett.*, 1996, **76**, 2934–2936.
149 B. Militzer and H. F. Wilson, *Phys. Rev. Lett.*, 2010, **105**, 195701.

150 C. Salzmann, I. Kohl, T. Loerting, E. Mayer and A. Hallbrucker, *J. Phys. Chem. B*, 2002, **106**, 1–6.
151 C. G. Salzmann, T. Loerting, S. Klotz, P. W. Mirwald, A. Hallbrucker and E. Mayer, *Phys. Chem. Chem. Phys.*, 2006, **8**, 386–397.
152 S. W. Peterson and H. A. Levy, *Acta Crystallogr.*, 1957, **10**, 70–76.
153 S. W. Rabideau, E. D. Finch, G. P. Arnold and A. L. Bowman, *J. Chem. Phys.*, 1968, **49**, 2514–2519.
154 S. J. La Placa and W. C. Hamilton, *J. Chem. Phys.*, 1973, **58**, 567–580.
155 B. Kamb, *Acta Crystallogr.*, 1964, **17**, 1437–1449.
156 B. Kamb, W. C. Hamilton, S. J. La Placa and A. Prakash, *J. Chem. Phys.*, 1971, **55**, 1934–1945.
157 B. Kamb, *Science*, 1965, **150**, 205–209.
158 P. W. Bridgman, *J. Chem. Phys.*, 1935, **3**, 597–605.
159 J. D. Jorgensen and T. G. Worlton, *J. Chem. Phys.*, 1985, **83**, 329–333.



 